Cancer Cell
Article

Promiscuous Mutations Activate the Noncanonical NF-κB Pathway in Multiple Myeloma

Jonathan J. Keats,[1,7] Rafael Fonseca,[1,7,*] Marta Chesi,[1] Roelandt Schop,[1] Angela Baker,[3] Wee-Joo Chng,[1] Scott Van Wier,[1] Rodger Tiedemann,[1] Chang-Xin Shi,[1] Michael Sebag,[1] Esteban Braggio,[1] Travis Henry,[1] Yuan-Xiao Zhu,[1] Homer Fogle,[1] Tammy Price-Troska,[2] Gregory Ahmann,[1] Catherine Mancini,[3] Leslie A. Brents,[6] Shaji Kumar,[2] Philip Greipp,[2] Angela Dispenzieri,[2] Barb Bryant,[5] George Mulligan,[5] Laurakay Bruhn,[4] Michael Barrett,[3] Riccardo Valdez,[1] Jeff Trent,[3] A. Keith Stewart,[1] John Carpten,[3] and P. Leif Bergsagel[1]
[1] Comprehensive Cancer Center, Mayo Clinic Arizona, Scottsdale, AZ 85259, USA
[2] Internal Medicine (Hematology), Mayo Clinic, Rochester, MN 55905, USA
[3] Hematological Malignancies Research Unit, Translational Genomics, Phoenix, AZ 85004, USA
[4] Agilent Technologies, Santa Clara, CA 95051, USA
[5] Millennium Pharmaceuticals, Cambridge, MA, 02139, USA
[6] Genetics Branch, National Cancer Institute, Bethesda, MD 20889, USA
[7] These authors contributed equally to this work.
*Correspondence: fonseca.rafael@mayo.edu
DOI 10.1016/j.ccr.2007.07.003

SUMMARY

Activation of NF-κB has been noted in many tumor types, however only rarely has this been linked to an underlying genetic mutation. An integrated analysis of high-density oligonucleotide array CGH and gene expression profiling data from 155 multiple myeloma samples identified a promiscuous array of abnormalities contributing to the dysregulation of NF-κB in approximately 20% of patients. We report mutations in ten genes causing the inactivation of *TRAF2*, *TRAF3*, *CYLD*, *cIAP1/cIAP2* and activation of *NFKB1*, *NFKB2*, *CD40*, *LTBR*, *TACI*, and *NIK* that result primarily in constitutive activation of the noncanonical NF-κB pathway, with the single most common abnormality being inactivation of *TRAF3*. These results highlight the critical importance of the NF-κB pathway in the pathogenesis of multiple myeloma.

INTRODUCTION

Multiple myeloma (MM) is a late stage B cell malignancy characterized by the accumulation of a monoclonal plasma cell population in the bone marrow. One-half of all patients have recurrent immunoglobulin gene translocations mediated by aberrant class switch recombination events, while the other half are hyperdiploid (Bergsagel et al., 1996; Fonseca et al., 2003b). However, both groups are characterized by dysregulation of a cyclin D gene, which appears to be an early and unifying event in MM pathogenesis (Bergsagel et al., 2005). A variety of secondary genetic events, associated with disease progression have been observed and include deletion of chromosome 13, amplification of chromosome 1q, deletion of *TP53*, activating point mutations of ras, and translocations of c-*myc* (Kuehl and Bergsagel, 2002). In addition to these known genetic events, the activation of NF-κB, by mechanisms that remain unclear, is thought to be a common event in MM. The activation of the NF-κB pathway by mutation has only been described in a single MM patient with an activating mutation of *NFKB2* (Fracchiolla et al., 1993). Nevertheless, the importance of this pathway in MM is highlighted by the clinical success of proteasome inhibitors (Richardson et al., 2003), which have been postulated to act principally by inhibiting NF-κB (Rajkumar et al., 2005).

The transcriptional regulation of NF-κB target genes is mediated by an array of homo- and heterodimers

SIGNIFICANCE

Activation of the canonical NF-κB pathway has been recognized in patients with multiple myeloma and attributed to interactions of the myeloma cell with the bone marrow microenvironment. We report a promiscuous array of mutations that result in constitutive activation of primarily the noncanonical NF-κB pathway in one-fifth of patients. The genetic selection of these mutations by the tumor cells highlights the critical importance of the NF-κB pathway in myeloma and suggests an important mechanism by which the tumor cells can begin to become independent of the microenvironment. Our results suggest that proteasome inhibitors that target the NF-κB pathway may be most effective in those patients with mutations causing constitutive activation of NF-κB.

containing p50 and p52, the active isoforms of NFKB1(p105) and NFKB2(p100) respectively (Hoffmann and Baltimore, 2006). The function of these dimers is dependent on ubiquitin mediated proteasomal degradation; however, the regulation of this process is different for dimers containing p50 or p52. The classical or "canonical" NF-κB pathway is negatively regulated by the inhibitors of NF-κB (IkBs), which retain p50-containing complexes in the cytoplasm to prevent their function as transcription factors. Therefore, the canonical pathway is not regulated by the processing of NFKB1 as the inactivation of the IkB complex is the rate-limiting step in the activation of the canonical pathway. In contrast, the "noncanonical" NF-κB pathway is solely regulated by the control of NFKB2(p100) processing to the active p52 isoform (Dejardin, 2006). The control of this process is dependent upon the presence of NF-κB-inducing kinase (MAP3K14/NIK), a protein that is normally undetectable as it is cotranslationally degraded in a TNF-receptor-associated factor 3 (TRAF3)-dependent manner (Liao et al., 2004). Consistently, *Traf3*$^{-/-}$ mice are characterized by constitutive processing of NFKB2 (He et al., 2006). Another TNF-receptor-associated factor, TRAF2, may also play a role in the control of NIK function as a conditional *Traf2* knock-out in B cells results in constitutive processing of NFKB2 (Grech et al., 2004).

The importance of the noncanonical NF-κB pathway in B cell development has been established in a number of model systems (Sen, 2006). First, the classical alymphoplasia mouse phenotype is caused by a missense mutation of *Nik* (Nik$^{aly/aly}$) that prevents the induction of NFKB2 processing (Shinkura et al., 1999). Additionally, *Nfkb2*$^{-/-}$ mice display a reduced B cell compartment, poor germinal center development, but a normal T cell compartment (Caamano et al., 1998; Franzoso et al., 1998). Conversely, transgenic mice expressing constitutively active isoforms of NFKB2, analogous to the ones identified in a variety of lymphoid malignancies (Neri et al., 1991), have an expansion of their B cell population (Ciana et al., 1997; Ishikawa et al., 1997).

In addition to their role in B cell homeostasis, the NF-κB pathways have been implicated in a wide variety of tumors; however, only a limited number of activating mutations have been reported (Courtois and Gilmore, 2006; Karin, 2006). Using a combined strategy of high-resolution array-based comparative genomic hybridization (aCGH) and gene expression profiling (GEP), we have identified abnormalities in a number of genes predicted to result in dysregulation of primarily the noncanonical NF-κB pathway. These mutations provide a genetic basis for the dysregulation of NF-κB in some cases of MM, and their genetic selection highlights the paramount importance of the NF-κB pathway in this disease.

RESULTS

aCGH Identifies Frequent Biallelic Deletions of NF-κB Regulatory Genes

In order to identify genetic abnormalities in MM we screened 62 patient samples and 46 human myeloma cell lines (HMCLs) originating from 42 individuals on a high density oligonucleotide aCGH platform with 42,896 features at an average genomic interval of ~35 kb (Barrett et al., 2004). We took a reductionist approach to the analysis of the aCGH data by focusing our analysis on biallelic/homozygous deletion events, which are intrinsically limited to small genomic regions but are likely to harbor tumor suppressor genes (see Figure S1 in the Supplemental Data available with this article online). To ensure that the observed biallelic deletions represented genuine events and not noise in the data or large common nucleotide variations (CNV) (Khaja et al., 2006; Redon et al., 2006), we first applied a circular binary segmentation algorithm (CBS) to the data (Olshen et al., 2004). The CBS algorithm provides a very stringent means of identifying biallelic deletions as it segregates chromosomal locations into regions with significant adjacent mean copy number changes. Although this reduced the resolution of the analysis from ~35kb to ~70kb, it significantly limits the number of false positive events. This analysis scheme identified 13 biallelic deletion events in 11 patients, encompassing 43 genes, and 80 biallelic deletions in 36 HMCLs, encompassing 148 genes, that do not represent physiological rearrangements of immunoglobulin loci or aberrations within previously characterized CNV regions (Table S1).

The only recurrent biallelic deletion identified by aCGH in our patient samples occurred at 14q32 and encompassed three potential target genes; *TRAF3*, *AMN*, and *CDC42BPB* (Figure 1 and Figure S2). Furthermore, this abnormality was one of only two identified in both our patient and HMCL data sets. We confirmed the biallelic deletions by cIg-FISH, and the minimally deleted region (MDR) was mapped by PCR in the two HMCLs with biallelic deletions to a genomic region of <48.8 kb using sequence tagged site (STS) and fine mapping primer pairs (Figure 1). This fine mapping approach eliminated *CDC42BPB* as a target gene of the deletion and thus only *TRAF3* or *AMN* remained as potential target genes. The remaining biallelic deletion identified in both of our data sets occurred at 11q22. This deletion was often quite large, ranging from 0.14–4.22 Mb in size; however, the MDR defined by aCGH was <109.05 kb in size and encompassed only 2 genes; *BIRC2*/cIAP1 and *BIRC3*/cIAP2 (Figure 1). As expected, the presence of a biallelic deletion correlated with reduced expression of the predicted target gene (Figure S3).

Interestingly, inactivation of TRAF3, cIAP1/2, and CYLD appears to be a common event in MM, as we identified a number of potential biallelic deletions in the publicly available data set from Carrasco et al. based on a correlation between the aCGH copy number and the expression level (Figure S4) (Carrasco et al., 2006). Combining these two patient data sets did not help to further refine the MDR encompassing TRAF3 or cIAP1/2; however, it did refine the MDR of the biallelic deletion we observed at 16q12 to a 72.05 kb region, which includes two genes, *CARD15* and *CYLD* (Figure S4).

Interestingly, 5/13 (38.5%) of the biallelic deletion events identified within our patient cohort contained

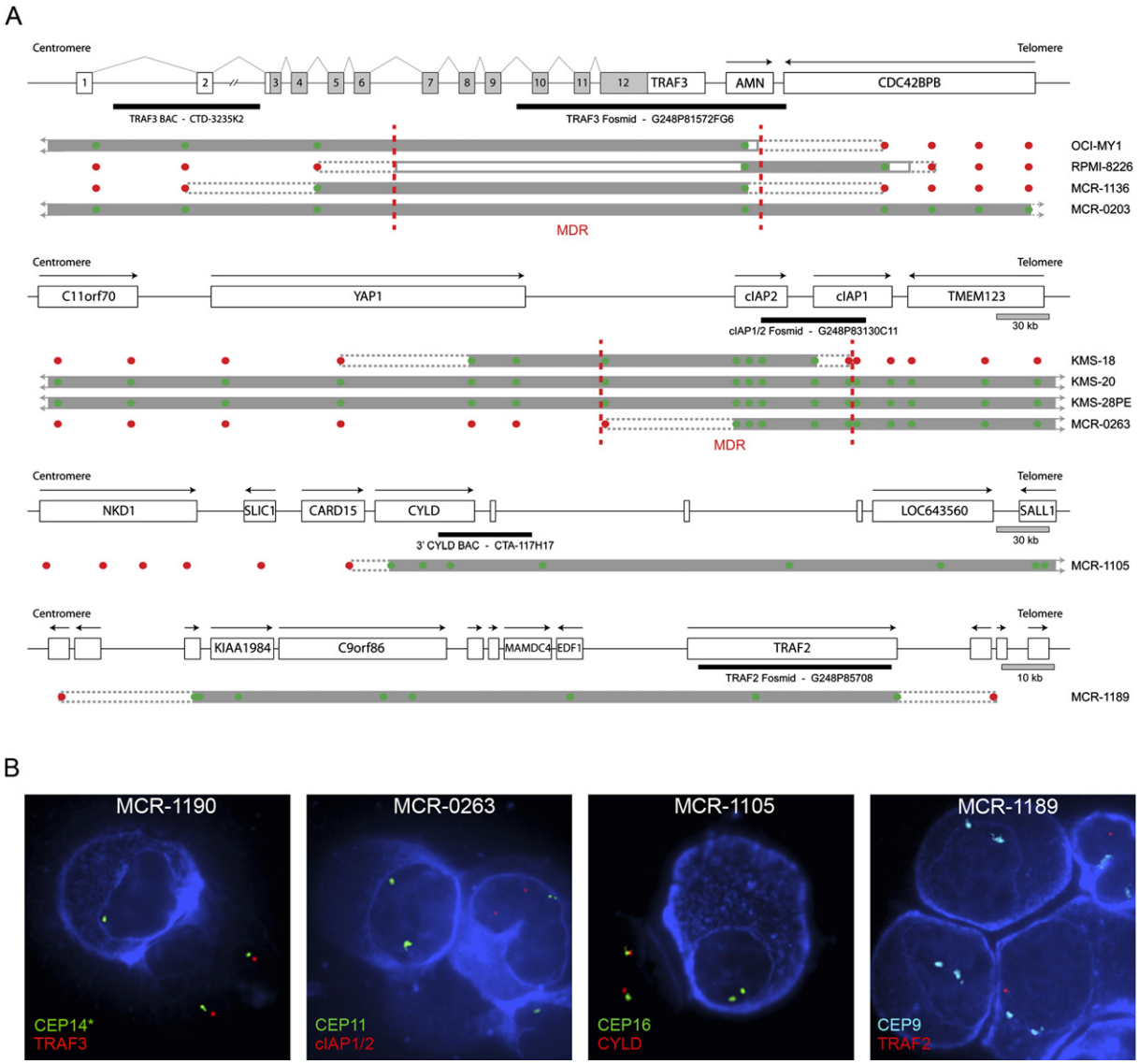

Figure 1. High Resolution aCGH Identifies Biallelic Deletions of NFKB Regulatory Genes

(A) The biallelic deletions (TRAF3, cIAP1 or cIAP2, CYLD, and TRAF2) predicted to target NF-κB regulatory genes identified in our 62 MM patient and 46 HMCL aCGH cohorts are shown. All of the maps except the TRAF3 map, which is drawn to relative scale so that the exon structure can be shown, are drawn to scale. Black arrows above each gene represent the direction of transcription. For TRAF3, the direction of transcription follows the numerical exon order and light gray exon regions indicate coding region. Each biallelic deletion is shown below the respective genomic map. Solid gray bars indicate regions of biallelic deletion, solid gray lines indicated regions of biallelic deletion mapped by PCR, and dashed gray lines indicate the region containing the breakpoint. The position and the copy number prediction of the aCGH probes contain on the microarray are indicated by red (one or more copies) or green (zero copies) dots. The position of probes used for cIg-FISH are shown below each genomic map. Dashed vertical red lines indicate the MDR identified by aCGH or PCR mapping.

(B) Representative images from the cIg-FISH validation of the aCGH findings are shown. Myeloma cells are identified by the blue cytoplasmic stain, which indicates the presence of either cytoplasmic kappa or lambda light chains. In the cIAP1/2 and TRAF2 panels, a macrophage (kidney-shaped nucleus) is shown that takes up the stain unspecifically. In the TRAF2 panel one of the three plasma cells shown still retains a copy of TRAF2, fitting the observed frequency of biallelic TRAF2 deletions observed in this patient sample.

potential target genes (*TRAF2*, *TRAF3*, cIAP1/2, and *CYLD*) associated with the regulation of the NF-κB signaling pathways. Based on these observations, we developed the working hypothesis that the frequent dysregulation of NF-κB signaling observed in MM is often the result of genetic abnormalities within the tumor cells.

Combined Analysis of GEP and aCGH Data Sets Identifies Additional Abnormalities within Regulators of the NF-κB Signaling Pathways

Our primary analysis of the aCGH data sets identified inactivation of 5 different genes involved in the NF-κB signaling pathways. To build on these observations, we combined

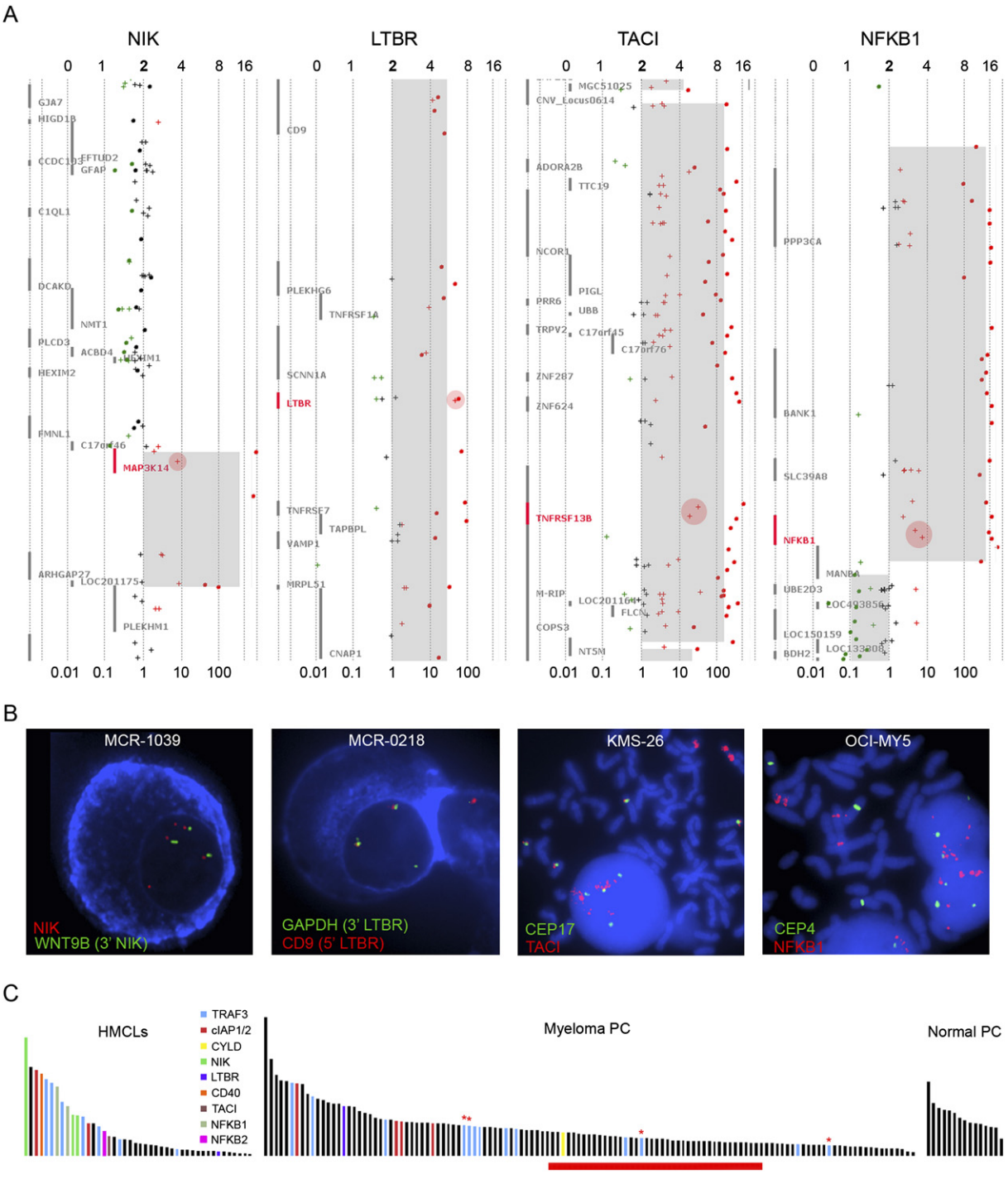

Figure 2. NFKB Related Genes with Spiked Expression Correlate with Genetic Abnormalities

(A) Representative plots indicating the regional copy number abnormality and corresponding gene expression level are shown. The gene of interest is highlighted in red on each plot. The predicted number of gene copies is indicated on the top of each panel and the median normalized expression level is shown at the bottom. Each aCGH probe is represented by a dot and the color of each dot corresponds to the log2 ratio of the probe; black dots, normal copy number (log2 ratio −0.25–0.25); green dots (log2 ratio < −0.25); red dots (log2 ratio > 0.25). The light gray region represents the mean copy number change identified by the CBS algorithm. Crosses indicate the gene expression probes for each gene and the log10 transformed expression levels are color coded to match the aCGH data. Pink circles highlight the expression probes corresponding to the gene of interest.

(B) Representative cIg-FISH images are shown that document the rearrangements of NIK and LTBR in MM patients, the duplication and insertion of CD40 into the Ig lambda locus, and the HSR containing TACI and NFKB1.

our aCGH and previously generated GEP data sets to identify additional abnormalities within genes involved in the NF-κB signaling pathways. A screen of our 125 patient and 44 HMCL GEP cohorts for spiked expression of genes involved in the regulation of NF-κB signaling identified overexpression of *MAP3K14*/NIK, *LTBR*, *CD40*, *TNFRSF13B*/TACI, and *NFKB1* (Figure 2 and Figure S3).

We identified the dysregulated expression of *NIK* in two HMCLs, L363 and EJM, that have previously been reported to overexpress NIK by either a t(17;22) translocation or amplification, respectively (C. Annunziata et al., 2006, Proc. Am. Assoc. Cancer Res., abstract). Because of these observations, we examined the aCGH data sets for abnormalities of the *NIK* locus. We confirmed the amplification in EJM and identified unbalanced rearrangements of *NIK* in one HMCL, JJN-3, and one patient, which were confirmed by cIg-FISH (Figure 2 and Figure S5).

We noted spiked expression of *LTBR* and *CD40* in both patient and HMCL cohorts. A >40-fold increase in the expression of *LTBR* was observed in one patient and in the HMCL FR4. For FR4, aCGH showed a significant amplification of the entire 12p chromosome arm, which was confirmed by FISH (Figure 2 and Figure S6). Interestingly, *LTBR* is one of only six genes on the entire arm with a >40-fold increase in expression. For the one patient with spiked *LTBR* expression, aCGH data was not available; however, FISH identified a single copy gain of the *LTBR* locus that is inserted at an unknown location (Figure S6). Within the surrounding region, only *LTBR* and *VAMP1* are overexpressed in this patient (Figure S6). For *CD40*, we identified one HMCL and two patient samples with spiked expression. By aCGH, the HMCL XG-2 contains a discrete two-copy gain of the *CD40* locus, which was confirmed by FISH and shown to be associated with the Ig-lambda locus (Figure S7). In the two patients with spiked *CD40* expression, aCGH data were not available and cIg-FISH did not detect a copy number variability or rearrangement of *CD40*.

We also detected the spiked expression of *TNFRSF13B*/TACI in the HMCL KMS-26 and *NFKB1* in OCI-MY5 and KMM-1. In both KMS-26 and OCI-MY5 the overexpression of *TACI* and *NFKB1* were mirrored by the presence of homologous staining regions containing the respective genes (Figure 2). In KMM-1, which had a 19-fold increase in the expression of *NFKB1*, a detectable alteration by aCGH was not identified. However, by FISH, an expression cloud was associated with a single *NFKB1* allele that disappeared following RNase treatment (Figure S8), suggesting that an unknown mechanism is driving the overexpression of *NFKB1* from a single allele in this HMCL.

Finally, we were able to correlate the presence of these diverse mutations with increased NF-κB transcriptional activity (Figure 2). The level of NF-κB-mediated transcriptional activity was determined based on a gene expression index developed from the HMCLs. We used an ANOVA test using the error estimate from a crossgene error model with multiple testing correction to identify six probe sets ($p < 0.05$) differentially expressed between the HMCLs with identified mutations compared to those without identified NFKB pathway mutations. We chose to remove two probe sets corresponding to HLA class II genes as their expression in patient samples may also derive from contaminating normal monocyte/macrophages and B cells. The mean expression level of the remaining four probe sets corresponding to CD74, IL2RG, and TNFAIP3 (2×) was used to represent the NFKB index. NF-κB transcriptional activity appeared to be high in all normal bone marrow plasma cells, likely due to stimulation from the surrounding microenvironment, but was variable in MM patients and HMCL. Clearly, the presence of mutations in the NF-κB pathways was associated with a higher level of NF-κB transcription activity in the HMCLs. This correlation was also observed in our MM patients, albeit to a lesser degree, but the correlation is also evident in other data sets (Figure S4). The reduced correlation between the NF-κB index and mutations seen in the patient data set may in part be due to the limitations inherent in the analysis of clinical material and to other sources of NF-κB activation originating from the bone marrow. However, in both data sets the association of these mutations with NF-κB transcriptional activity is not likely to result from chance alone as a hypergeometric distrubution test, a statistical test commonly used in enrichment analysis, returned p values of 0.009 and 0.04, respectively.

FISH Validation of Genetic Abnormalities within the NF-κB Signaling Pathways

To determine the frequency of *TRAF3* deletions, we blindly screened a large cohort of MM patients by cIg-FISH, including 60 patients initially screened by aCGH and 98 additional patients. We identified 6 (3.8%) patients with biallelic *TRAF3* deletions and 19 (12.0%) patients with a single *TRAF3* allele (Table 1). There was almost complete concordance between the FISH and aCGH results with the exception of two patients in whom the presence of the biallelic deletion was heterogeneous by FISH and below the detection limit of aCGH. However, in both these cases, aCGH demonstrated a clear loss of chromosome 14, which suggests that the biallelic deletions seen by FISH occurred after the q-arms of chromosome 14 were lost.

To systematically screen the limited patient material for deletions of *TRAF2*, cIAP1/2, and *CYLD* by cIg-FISH, we selected patients for screening based on either 1N copy number of these genes, as determined by aCGH or a median normalized expression below 0.4. This process identified three additional patients with cIAP1/2 deletions and one additional patient with a *CYLD* biallelic deletion

(C) Histogram plots of the NFKB index from normal PC, myeloma PC, and HMCL are shown and indicate the correlation between the NFKB index and the presence of an abnormality in the NF-κB pathways. The red bar below the index corresponds to the predicted transition point between processed versus unprocessed NFKB2. The red asterisks identify samples with questionable TRAF3 inactivation due to either a heterozygous mutation call by sequencing or a biallelic deletion in less than 25% of the plasma cells.

Table 1. Frequency of Genomic Deletions within NF-κB Related Genes

Gene	Sample	Assay	n	Number of Gene Copies		
				2N/3N/4N	1N	ON
TRAF3	HMCL	aCGH	42[a]	29 (69.1)	10 (23.8)	3 (7.1)
	patients	FISH	158	133 (84.2)	19 (12.0)	6 (3.8)[b]
		aCGH	62	54 (87.1)	6 (9.7)[b]	2 (3.2)
		total	160	134 (83.7)	19 (11.9)	7 (4.4)
TRAF2	HMCL	aCGH	42	35	7	0
	patients	FISH[e]	7	6	0	1
		aCGH	62	60 (96.8)	1 (1.6)	1 (1.6)
cIAP1/2	HMCL	aCGH	43[c]	36	7	3
	patients	FISH[f]	15	11	0	4
		aCGH	62	60	1	1
CYLD	HMCL	aCGH	43[d]	34 (79.1)	9 (20.9)	0
	patients	FISH[g]	30	13	15	2
		aCGH	62	50 (80.7)	11 (17.7)	1 (1.6)

A total of 46 HMCL were screened by aCGH; however, the 46 HMCL only represent 42 individuals because some of the lines originate from the same individual. The following HMCL were screened: ANBL-6, Delta47, EJM, FLAM-76, FR4, H1112, INA-6, JIM3, JJN-3, JK-6L Schon, Karpas620, KHM-11, KHM-1B, KMM-1, KMS-11, KMS-12BM, KMS-12PE, KMS-18, KMS-20, KMS-26, KMS-28BM, KMS-28PE, KMS-34, L363, LP-1, MM.1R, MM.1S, MM-M1, NCI-H929, OCI-MY1, OCI-MY5, OCI-MY7, OPM-1, OPM-2, PE-1, PE-2, RPMI-8226, SACHI, SKMM-1, SKMM-2, U266, UTMC-2, XG-1, XG-2, XG-6, and XG-7.

[a] Although the aCGH defined copy number of the *TRAF3* locus in KMS-11 is 1N it has been placed in the ON category as a biallelic deletion of exon 7, an unrepresented region on the aCGH chip, was discovered during exon resequencing.

[b] Two patients are differentially represented in the 1N and ON categories between the FISH and aCGH result categories. In both cases, the biallelic deletion of *TRAF3* was seen in a subpopulation of the light-chain-selected plasma cells while the remaining populations show only a single copy of *TRAF3*. Because of this mixed population both patients are characterized as 1N by aCGH.

[c] The total number of HMCL is noted as 43 as KMS-28PE shows a biallelic deletion of *cIAP1* and *cIAP2*, while the sister HMCL KMS-28BM, derived 1 month later (T. Otsuki, Personal Communication), shows a 1N copy number.

[d] The total number of HMCL is noted as 43 as KMS-12BM shows a single copy of *CYLD* while the sister HMCL KMS-12PE, derived 2 months earlier (T. Otsuki, Personal Communication), shows the normal 2N copy number.

[e] FISH confirmed the biallelic *TRAF2* deletion observed in one patient by aCGH.

[f] We screened a panel of patients for *cIAP1* and *cIAP2* abnormalities based on their low expression of *cIAP1* as detected by GEP, or the prediction of a 1N copy number by aCGH. This panel includes 13 patients who were not screened by aCGH. FISH confirmed the biallelic deletion observed in one patient by aCGH.

[g] We screened a panel of patients for *CYLD* abnormalities based on their low expression of *CYLD*, as detected by GEP, or the prediction of a 1N copy number by aCGH. This panel includes nine patients for whom aCGH data is not available. FISH confirmed the biallelic CYLD deletion observed in one patient by aCGH.

(Table 1). No additional cases were identified with *TRAF2* deletions. In summary, we identified biallelic deletions of *TRAF2*, *TRAF3*, *CYLD*, or cIAP1/2 in 14/167 patients and of TRAF3, *CYLD*, or cIAP1/2 in 10/67 in the Carrasco data set. We believe that the cumulative incidence of these abnormalities is underestimated as only TRAF3 was studied in the majority of patients due to the limited availability of patient material.

Sequencing Identifies Mutations of *TRAF3* and *CYLD*

To determine the overall rate of inactivation of the identified target genes, we performed bidirectional sequencing of the coding regions of these genes. The individual coding exons and flanking mRNA splicing sites of *TRAF3* were sequenced in 62 patients and in the entire panel of 46 HMCLs. Through this process, we found a third HMCL, KMS-11, with a biallelic deletion of *TRAF3* originating from two independent deletions overlapping at exon 7 (data not shown). In the remaining HMCLs, we found four independent mutations including three frameshifts and one in-frame deletion, which are predicted to inactivate *TRAF3* (Figure 3, Table 2, and Table S2). All HMCL, except the three HMCLs with biallelic deletions, expressed detectable full-length *TRAF3* mRNA transcripts and no discernable transcript length variations, suggestive of unknown alternative splicing events, were observed.

We sequenced 49 randomly selected patient samples for *TRAF3* and identified three different mutations (one nonsense and two missense). Subsequently, *TRAF3* sequencing was extended to an additional 13 patients in whom LOH of the TRAF3 locus had been characterized by aCGH or cIg-FISH, and DNA or RNA was available for sequencing. This process identified seven additional abnormalities within the coding region of *TRAF3*, including

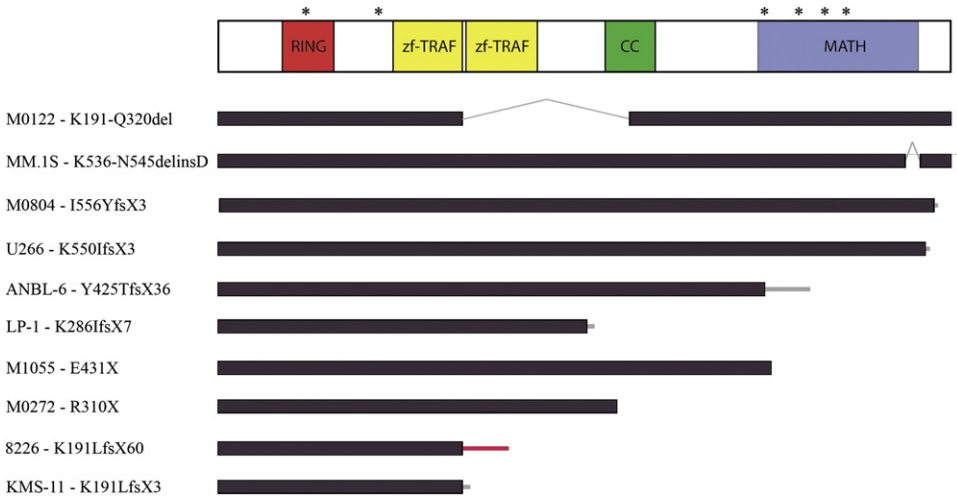

Figure 3. Sequencing Identifies Mutations in the Coding Region of *TRAF3*

A scale diagram of the *TRAF3* polypeptide and the known protein domains identified by the SMART prediction tool are shown. Asterisks above the diagram note the position of the identified missense mutations (H70Y, R118W, Q430R, G462A, G480E, and F490C) while the nonsense, frameshift, and deletion mutations and the associated polypeptide effects are shown below as black bars. Black bars represent normal coding regions, gray lines indicate deleted regions, and thin bars represent the position of a frameshift and the length of translation before a stop codon is encountered. The thin gray bars indicated the translation of sequence originating within the *TRAF3* locus while red bars indicate the translation of regions outside of the *TRAF3* locus.

one nonsense, one frameshift, and four missense mutations along with one large deletion (Table 2 and Table S2). All of the missense mutations occur at amino acids conserved throughout vertebrate evolution (Figure S9), suggesting their functional relevance. Surprisingly, one of the patients with a subpopulation of cells with a biallelic deletion of *TRAF3*, MCR-0319, also had a missense mutation, which inactivates the RING domain of TRAF3 (Figure 3 and Figure S9). A domain recently shown to be essential for the negative regulation of NIK by TRAF3 (He et al., 2007). Altogether, TRAF3 is inactivated in 17% of HMCL and approximately 12.3% of MM patients by either biallelic deletion or by LOH associated with an inactivating mutation.

We sequenced the coding exons of *CYLD* in 11 patients with either low levels of *CYLD* expression or LOH and identified a single nonsense mutation, S265X, in one patient sample with LOH (Table 2 and Table S2). No mutations were identified in HMCLs with LOH of *CYLD* (Table 2). In the HMCL JK-6L, we identified a frameshift mutation in NFKB2, which was investigated based on the presence of an abnormal immunoblot band. In the only patient with LOH of the cIAP1/2 locus, we did not detect an abnormality within the coding region of *cIAP1* or *cIAP2*.

Table 2. Inactivation of NF-κB Pathway Genes

Gene	Sample	Samples Sequenced	Inactivating Mutations			Inactivation
			2N/3N/4N	1N	ON	
TRAF3	HMCL	41[a]	1/29 (3.4)	4/10 (40.0)	0/3	7/42 (16.7)
	patients	62[b]	1/43 (2.3)	8/16 (50.0)	1/3	12/62 (19.4)[c]
CYLD	HMCL	16	0/7	0/9		0/16
	patients	11	0/6	1/5		1/11

An additional 15 patients were partially sequenced for *TRAF3*, *cIAP1*, *cIAP2*, and *CYLD* abnormalities at the University of Toronto. A single patient harbored a heterozygous nonsense mutation (c.900C > T, Q183X) of *TRAF3*. In addition to the observed mutation, a number of previously undocumented SNP were identified in *TRAF3*, *CYLD*, *cIAP1*, and *cIAP2*.

[a] OCI-MY1 was not sequenced because the entire *TRAF3* locus is deleted.

[b] An initial panel of 49 unselected patients was screened for *TRAF3* coding mutations, in which three mutations were identified. Subsequently, a selected population of 13 patients with a single *TRAF3* allele, or mixed population of 1N and ON defined by FISH, was screened for *TRAF3* mutations if template material was available for cDNA or DNA based sequencing approaches, and this identified seven additional mutations.

[c] The expected frequency of TRAF3 inactivation by mutation or biallelic deletion after a 1N selection bias correction is ~12.3%. Correction Calculation = Biallelic Frequency + (1N Frequency × 1N Mutation Frequency) + (2N/3N/4N Frequency × 2N/3N/4N Mutation Frequency).

In summary, our comprehensive genetic screen identified a promiscuous array of genetic alterations that are predicted to result in constitutive activation of NF-κB signaling. When all of the biallelic deletion events, mutations, and gene rearrangements of *TRAF2*, *TRAF3*, cIAP1/2, *CYLD*, *NIK*, *LTBR*, *CD40*, *TACI*, *NFKB2*, and *NFKB1* are combined, at least 28/167 (17%) MM patients and 19/46 (41.3%) HMCL have an abnormality that leads to the dysregulation of NF-κB signaling.

Genetic Alterations of TRAF3, BIRC2, BIRC3, CD40, NIK, TACI, and LTBR Correlate with the Processing of NFKB2

To determine if the genetic aberrations we identified were associated with constitutive processing of NFKB2, we screened the panel of HMCLs for the processing of p100 to p52 (Figure 4 and Table S3). We identified constitutive NFKB2 processing in HMCLs with abnormalities of *TRAF3*, cIAP1/2, *NIK*, *CD40*, *LTBR*, and *TACI*. As expected, the HMCLs that overexpress NIK or have TRAF3 inactivating abnormalities had constitutive NFKB2 processing while HMCL overexpressing NFKB1, OCI-MY5, and KMM-1 did not have detectable NFKB2 processing. The constitutive processing of NFKB2 from p100 into p52 correlates with both a high NFKB index and the detection of the normally cytoplasmic NFKB2 in the nucleus (Figure 4) (Table S3). In addition, the HMCLs with inactivation of TRAF3 and rearrangements of *NIK* were associated with detectable levels of NIK protein. Surprisingly, we also found high levels of NIK and constitutive processing of NFKB2 in HMCLs with cIAP1/2 biallelic deletions (Figure 4). The constitutive processing of NFKB2 seen in these HMCLs must be linked to the absence of cIAP1 and/or cIAP2 as the isogenic HMCL pair (KMS-28BM/PE), which were independently derived from the bone marrow or the pleural effusion of the same patient and share virtually identical genomes, except for their difference in the presence (KMS-28BM) or absence (KMS-28PE) of cIAP1/2 also process NFKB2 differently. In this pair, the absence of cIAP1/2 is associated with increased levels of NIK protein and constitutive NFKB2 processing (Figure 4). As all of our biallelic deletions encompassed both cIAP1 and cIAP2 and we did not identify a mutation in either gene, we cannot determine if the loss of one or both is associated with NFKB2 processing.

Surprisingly, 2 of 3 HMCLs, L363 and EJM, with NIK abnormalities did not have detectable TRAF3 protein. However, the third cell line, JJN-3, which has a NIK rearrangement deleting the TRAF3 interaction domain (M. Kuehl, personal communication), had high levels of TRAF3 protein. Although it is known that TRAF3 regulates NIK protein stability, these two observations suggest that a direct NIK-TRAF3 interaction may also regulate TRAF3 protein levels. Furthermore, the high levels of TRAF3 in the cell lines lacking cIAP1/2 suggest this may occur in a cIAP1/2-dependent manner.

In conclusion, the majority of the genetic abnormalities we identified in our cohort of MM patients and HMCLs have highlighted a multifaceted mechanism that constitutively activates the noncanonical NF-κB pathway. The selection of so many mutations in a single pathway highlights its importance in myelomagenesis and identifies a potential tumor specific vulnerability.

Characterization of TRAF3 as a Tumor Suppressor Gene

Since TRAF3 inactivation represented the most common abnormality we identified in the noncanonical NF-κB pathway in MM, we investigated its potential role as a tumor suppressor. We constructed an adenovirus capable of high efficiency infection, which expresses wild-type TRAF3 and used it to reintroduce $TRAF3^{wt}$ into the HMCLs with TRAF3 abnormalities. Based on the well-documented role of TRAF3 as a negative regulator of NFKB2 processing, we assayed its effects on p100 processing. In all of the HMCLs with TRAF3 abnormalities, the reintroduction of $TRAF3^{wt}$ was associated with an inhibition of NFKB2 processing from p100 to p52 (Figure 5). In addition, overexpression of TRAF3 in the HMCL L363, which overexpresses NIK due to an IgL translocation, leads to a marked inhibition of NFKB2 processing.

The involvement of TRAF3 in the regulation of NIK stability and the subsequent p100 processing is well documented; however, a role in oncogenesis has never been reported. We hypothesized that the inactivation of TRAF3 would provide cells with a selective growth advantage. As we predicted, the reintroduction of $TRAF3^{wt}$ caused a significant growth delay in 4/5 HMCL associated with G0/G1 cell cycle arrest and a significant increase in apoptosis (Figure 5). The control HMCLs, OCI-MY5 and OPM-1, that do not have constitutive processing of NFKB2 were not affected by TRAF3 overexpression.

Inactivation of TRAF3 Is Associated with Poor Response to Dexamethasone and a Good Response to Proteasome Inhibitors

Proteasome inhibitors are a novel class of anticancer agents with remarkable clinical activity in MM (Richardson et al., 2003). Although they presumably have multiple mechanisms of action, the principally defined mechanism has been postulated to be the inhibition of NF-κB signaling. We hypothesized that MM with constitutive activation of the noncanonical pathway would be particularly sensitive to proteasome inhibition. Unfortunately, we could not test this hypothesis in the HMCLs, which are uniformly sensitive to proteasome inhibitors and differ from patients in a number of ways, most notably proliferation. Instead we examined a GEP data set of relapsed/refractory MM patients randomly assigned to treatment with either dexamethasone or the proteasome inhibitor bortezomib (Mulligan et al., 2007). As we could not screen these patient samples for mutations, we used an ROC analysis of our patient data set to identify a median normalized expression cutoff of 0.6 as the best crossover point between sensitivity and specificity and used this value as a surrogate means of identifying patients who likely have TRAF3 abnormalities. In our data set, 17/25 patients with *TRAF3* expression below 0.6 lack functional TRAF3. Using this

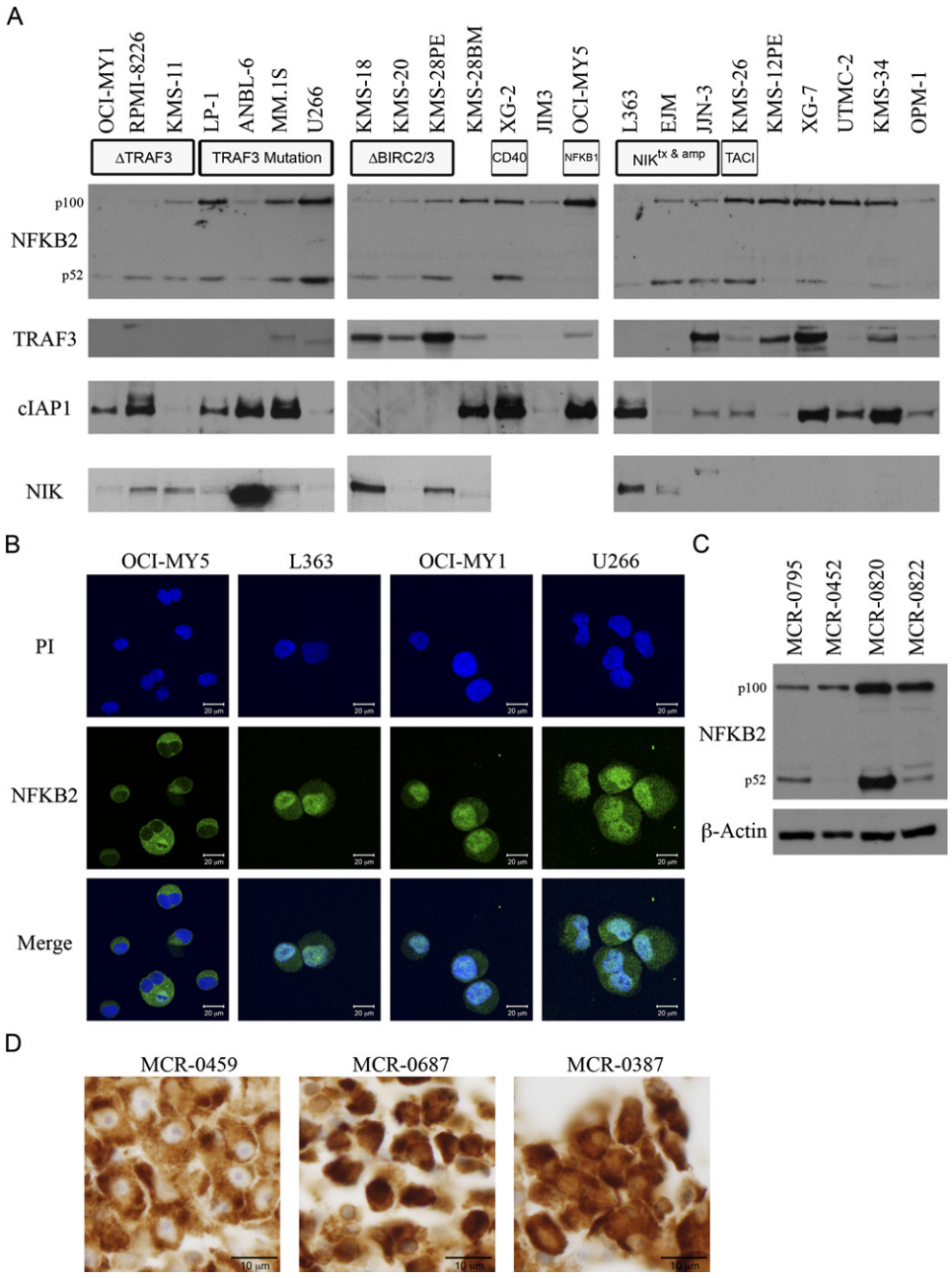

Figure 4. Mutations in the Noncanonical NF-κB Pathway Correlate with Processing of NFKB2 and the Presence of NFKB2 in the Nucleus

(A) Immunoblots for the proteins of interest from the indicated HMCLs are shown. The three vertical panels are separated into a TRAF3, cIAP1, and NIK panel plus additional HMCL when possible. For the NFKB2, TRAF3, and NIK blots, L363 and OPM-1 were included on the ends of each blot to serve as positive and negative controls and to ensure equivalent exposure between each panel. The cIAP1 blot for L363 has been taken from another gel as we had included KMS-18 as a negative control in all of the blot panels, and this prevented L363 from being included. In all instances the biallelic deletion of *TRAF3* or *cIAP1* corresponds with the complete absence of a detectable protein product.

(B) The association between processing of NFKB2 and nuclear localization of NFKB2 was confirmed by immunofluorescence of HMCL without NFKB2 processing (OCI-MY5) compared to those with constitutive NFKB2 processing (L363, NIK overexpression; OCI-MY1, TRAF3 biallelic deletion; and U266, homozygous TRAF3 mutation).

(C) An NFKB2 immunoblot confirms the existence of NFKB2 processing in MM patient samples and shows a correlation between the processing ratio (left-right; positive, negative, positive, negative) and NFKB index (left-right; 1.07, 0.45, 1.26, 0.56).

(D) Immunohistochemistry of patients with a low (MCR-0459) or high (MCR-0687) NFKB index, along with a patient with a TRAF3 biallelic deletion (MCR-0387), confirms the association between a high NFKB index or TRAF3 mutation and nuclear NFKB2. The images are representative of the five patient samples tested from each category. All core biopsies but one with sufficient plasma cells for scoring correlated with expectations of nuclear NFKB2 in TRAF3 mutants or samples with high NFKB index while samples with no known mutation and a low NFKB index had cytoplasmic NFKB2.

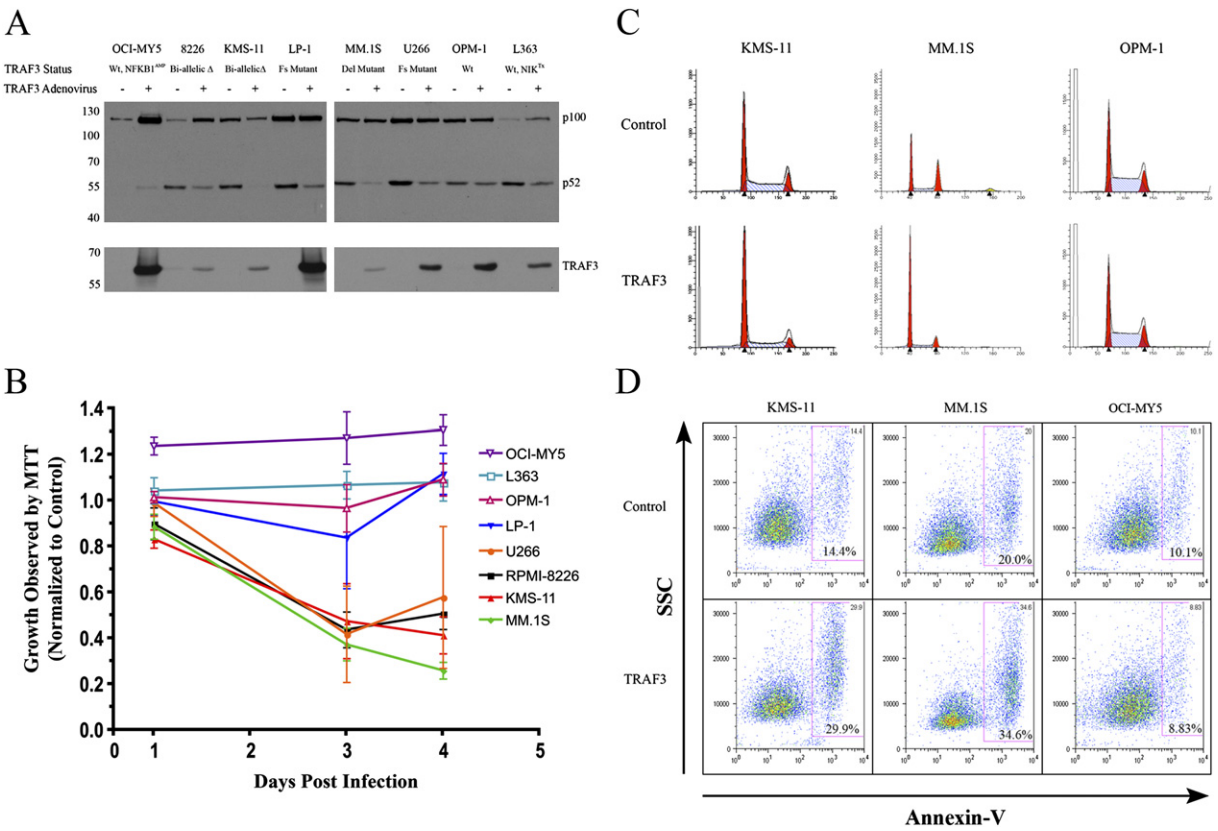

Figure 5. TRAF3 Reintroduction Inhibits NFKB2 Processing and Causes a Growth Arrest

The effects on HMCLs infected with an adenovirus expressing either EGFP and TRAF3^{WT} or EGFP alone are shown.

(A) Immunoblot showing the inhibition of p100 processing 48 hr postinfection.

(B) Effects of TRAF3^{WT} expression on MTT-defined cell growth. Infected cells were seeded 24 hr postinfection and the effects on cell growth we compared to control infections at 72 hr and 96 hr postinfection. Cells were seeded at specific densities to ensure that the cells infected with the EGFP-expressing control virus remained in the exponential phase of the growth curve at both time measurements. Error bars represent the standard deviation.

(C) Effect of TRAF3^{WT} expression on the cell cycle status of selected HMCL 48 hr postinfection. The scale for each plot has been normalized for each HMCL.

(D) TRAF3^{WT} reintroduction is associated with a significant increase in apoptosis as measured by Annexin-V staining.

cutoff, 39/193 (20%) patients likely have a *TRAF3* abnormality, a rate similar to that observed in our cohort. In this clinical trial data set 2/20 (10%) patients with low levels of *TRAF3* responded to dexamethasone whereas 17/19 (89%) responded to bortezomib. This was accompanied by a prolongation of progression-free-survival (PFS) from 83 to 193 days ($p < 0.0001$). For patients with levels of TRAF3 above 0.6, 15/50 (30%) responded to dexamethasone and 42/104 (40%) to bortezomib, with no difference in PFS (140 versus 145 days) (Figure S10). These results suggest that constitutive activation of the noncanonical NF-κB pathway by inactivation of TRAF3 is associated with dexamethasone resistance and proteasome inhibitor sensitivity. The resistance to dexamethasone was unexpected but may relate in part to the fact that one of the mechanisms of action of glucocorticoids targets only the canonical NF-κB pathway. It has been reported that hormone-bound glucocorticoid receptor is recruited to promoters by binding relA-containing dimers, thereby disrupting relA's interaction with certain coactivators(Hoffmann and Baltimore, 2006). One would anticipate that this mechanism would be of little consequence in patients with constitutive activation of the noncanonical NF-κB pathway. Using the top and bottom third of the NFKB index to discriminate patients shows that patients in the high index group have a better response rate to bortezomib, although no difference in PFS. These results suggest that bortezomib may be most effective in patients with constitutive noncanonical NF-κB activation (as seen in patients with inactivation of TRAF3).

DISCUSSION

Our integrated analysis of high-resolution aCGH and GEP identified a plethora of genetic abnormalities resulting in the activation of the NF-κB signaling pathways. We observed overexpression and/or gain-of-function mutations in *NIK*, *NFKB2*, *NFKB1*, *CD40*, *LTBR*, and *TACI*, which are

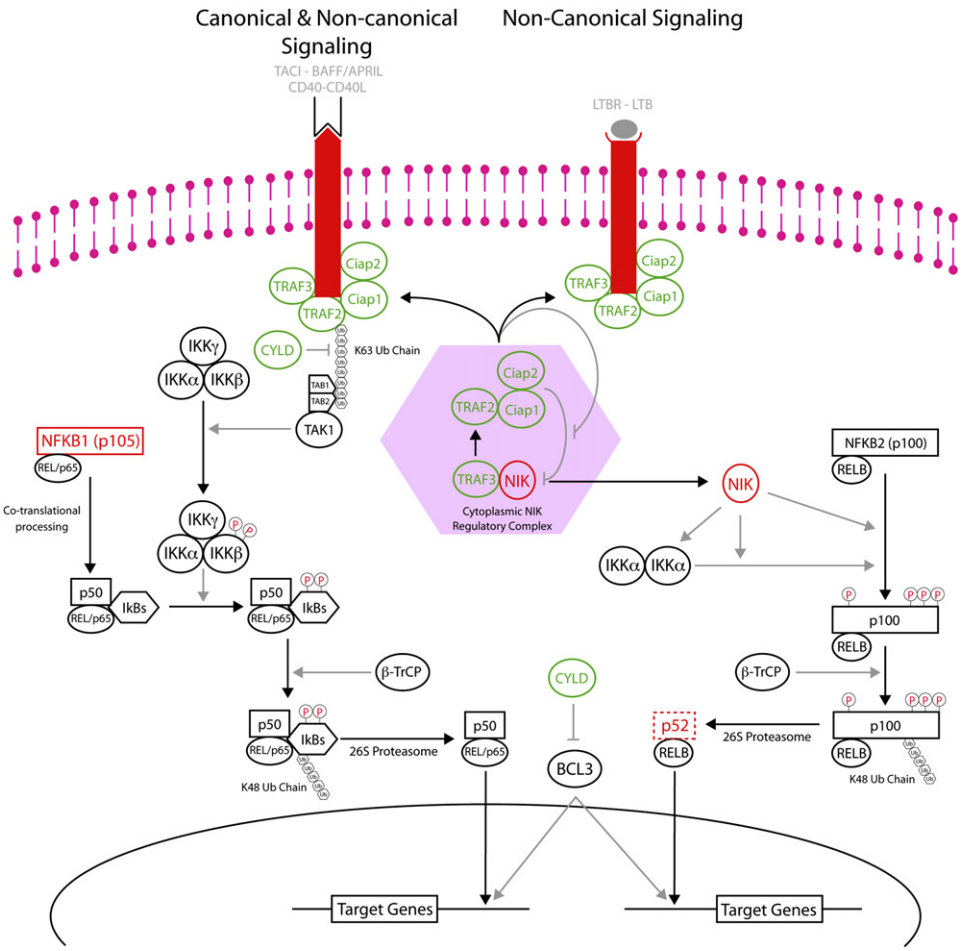

Figure 6. Proposed Model Indicating the Effects of the Identified Abnormalities on the Noncanonical NF-κB Pathway

The genes with inactivating abnormalities (*TRAF2*, *TRAF3*, *cIAP1*, *cIAP2*, and *CYLD*) are indicated by green objects while the genes with activating abnormalities (*LTBR*, *TACI*, *CD40*, *NIK*, and *NFKB2*) are indicated by red objects. Based on our observations and those from other groups, we propose the existence of a cytoplasmic NIK regulatory complex, shown in the light red hexagon, that is dependent on TRAF2, TRAF3, cIAP1, and/or cIAP2.

all positive regulators of NF-κB signaling. Furthermore, we identified inactivating abnormalities of *TRAF3*, *cIAP1*/*cIAP2*, *CYLD*, and *TRAF2*, which are negative regulators of the NF-κB pathways. Importantly, these observations provide valuable insight into the significant contribution of the noncanonical NF-κB pathway in the pathogenesis of MM. In the course of this study, we have made several compelling observations. First, TRAF3 is a tumor suppressor gene that is inactivated at a frequency greater than any other known tumor suppressor in MM. Furthermore, its reduced expression correlates with dexamethasone resistance and bortezomib sensitivity. Second, inactivation of *cIAP1* and/or *cIAP2* by biallelic deletion is associated with an activation of the noncanonical NF-κB pathway. Third, we found an inactivating mutation in *CYLD* associated with LOH, suggesting that *CYLD*, the causative gene in cylindromatosis, may play a role in the development of MM.

To date, the dysregulation of NF-κB signaling observed in MM has largely been linked to ligand-dependent interactions occurring in the bone marrow. We have found that plasma cells isolated from the bone marrow of healthy individuals have an elevated NF-κB transcriptional index, suggesting that activation of NF-κB is a physiological feature of these cells. The ligand-dependent NF-κB stimulation of normal plasma cells likely serves to regulate the growth and survival of these cells within the confines of the bone marrow compartment. We propose that the acquisition of mutations reported here results in the accumulation of malignant plasma cells beyond this physiological control. Our results suggest a mechanism by which MM cells can overcome these limitations through the acquisition of mutations that result in constitutive and ligand-independent activation of the noncanonical NF-κB pathway.

The regulation of the noncanonical NF-κB pathway is absolutely dependent on the presence of NIK that, although constitutively transcribed, is normally undetectable in the absence of receptor engagement (Qing et al., 2005), which sequesters the normally cytoplasmic localized TRAF2, TRAF3, and cIAP1/cIAP2 proteins to the

plasma membrane (Fotin-Mleczek et al., 2004; Vischioni et al., 2004). Based on our observations, we predict the existence of a cytoplasmic complex regulating the cotranslational degradation of NIK, which relies on the presence of TRAF2, TRAF3, cIAP1, and/or cIAP2 (Figure 6). We hypothesize a mechanism in which, in the absence of stimuli, cytoplasmic TRAF3 scavenges the cytoplasm for NIK, which is then recruited to complexes containing TRAF2, cIAP1, and cIAP2 for degradation. Upon receptor engagement, these regulators are sequestered to the plasma membrane (Kuai et al., 2003), leading to NIK stabilization. We believe that any mutation affecting the binding of these regulators to each other and to NIK would result in NIK stabilization. In conclusion, the genetic abnormalities we have identified are expected to contribute to the constitutive processing of NFKB2 by either inhibiting the function of the NIK regulatory complex (*TRAF2*, *TRAF3*, *cIAP1*, and/or *cIAP2* abnormalities), bypassing or overwhelming the NIK regulatory complex (*NIK* or *NFKB2* abnormalities), or by recapitulating the natural process that inactivates the NIK regulatory complex by recruiting the various constituents to the plasma membrane (*LTBR*, *TACI*, and *CD40* overexpression).

While TRAF3 is a recognized regulator of the noncanonical NF-κB pathway, it has never been implicated in a malignant process. In this study, we have found that TRAF3 is inactivated at a frequency greater than that of any other tumor suppressor in MM. Given this frequency, we suspect that other malignancies might harbor TRAF3 abnormalities. In fact, 21 of 83 cell lines derived from a variety of malignancies lacked detectable TRAF3 by immunohistochemistry (Zapata et al., 2000).

In conclusion, we have identified a promiscuous array of mutations that result in the constitutive activation of the noncanonical NF-κB pathway in approximately 20% of MM patients. The remarkable activity of bortezomib in patients with inactivation of TRAF3 suggests that one of its most important mechanisms of action in MM is the inhibition of the noncanonical NF-κB pathway. Therefore, we believe that the specific targeting of the direct NFKB2 regulators NIK and IKKα may be particularly effective in MM treatment.

EXPERIMENTAL PROCEDURES

Sample Preparation

Bone marrow aspirates were collected from 167 MM patients (28 SMM and 139 overt MM). All patients provided written informed consent approving the use of their samples under Institutional Review Board approval. The BM aspirates were treated with ACK lysis buffer to remove red blood cells and plasma cells were isolated using immunomagnetic sorting on a Miltenyi AutoMacs or StemCell Robocept with anti-CD138 antibodies. We enumerated 100 nucleated cells for kappa and lambda staining to determined the purity of the CD138 sorts and found that the mean plasma cell purity (kappa and lambda) was 95.5% (Median 96.0, range 69%–100%) while the mean clonal purity (clinical light chain) was 92.7% (Median 95.0, range 54–100). Isolated cells were suspended in TRIzol (Invitrogen) and stored at −80°C for long-term storage. Nucleic acids were isolated from TRIzol following the protocol supplied by the manufacturer. The RNA used for gene expression profiling was cleaned up using the QIAGEN RNeasy kit, while the DNA used for aCGH was cleaned up by phenol-chloroform extractions after RNase and proteinase K treatments. The HMCLs were maintained as previously described (Bergsagel et al., 1996).

Microarray Experiments

GEP of the patient samples was performed on U133A genechips following the manufacturer's suggested protocol, while the 46 HMCL samples were done on U133 Plus 2.0 (Affymetrix, Santa Clara, CA) as previously described (Carrasco et al., 2006). Median normalized gene expression profiles were analyzed using GeneSpring (Agilent).

High-resolution aCGH was performed on 62 patient and 46 HMCL samples with the Human Genome 44B microarray (Agilent Technologies) following the protocol suggested by the manufacturer. Briefly, 800 ng of test (MM CD138+ cells or HMCL) and normal female reference (Promega) were directly labeled with either Cy5 or Cy3 using the BioPrime Array CGH Genomic Labeling Module (Invitrogen) and purified using Vivaspin 500 spin columns (Sartorius). The hybridization reactions containing equal amounts of test and reference DNA were hybridized to the microarray at 65°C for 40 hr in a rotation oven at 20 rpm. The slides were washed and then scanned with the Agilent G2505B DNA microarray scanner. The microarray images were analyzed using Feature Extraction software V8.1 (Agilent) and Log2 transformed ratio data was analyzed with GeneSpring GX V7.3.1 and CGH Analytics V3.4.27 (Agilent).

Sequencing

When possible individual coding exons were amplified from 10 ng of CD138 purified plasma cell DNA in 25 μl reactions using Platinum Taq DNA Polymerase (Invitrogen, Carlsbad CA) and M13 tagged exon specific primes (Table S4). Alternatively, overlapping segments of the entire open reading frame were amplified from RNA converted to cDNA using Superscript II and oligo dT17. Sequencing reactions were carried out using Big Dye V3.1 and capillary electrophoresis was performed on an ABI 3730 at the Mayo Clinic or TGEN sequencing core facilities. DNA sequences were analyzed using Sequencher V4.5.

FISH

The cIg-FISH method was performed as previously described (Fonseca et al., 2003a). Briefly, probes specific to each region of interest were selected using the UCSC genome browser and the specific positions were confirmed by manual mapping of the available end sequences to data available from HGB 36.2. The selected BAC clones were purchased from Invitrogen and the Fosmid clones were ordered from the BACPAC Resources Center. The specificity of each probe was confirmed by hybridization to normal metaphase preparations to confirm chromosome and band specificity, and gene specific PCR was used to confirm the presence of DNA sequence corresponding to the specific region of interest. A list of the various FISH probes is provided in Table S5 and a map of the different regions is provided in Figure S11.

Immunoblotting, Immunofluorescence, and Immunohistochemistry

Total cellular extracts were prepared from freshly isolated HMCLs using 10× Cell Lysis Buffer (Cell Signaling Technologies) supplemented with 1 mM PMSF. Protein samples were resolved on 7.5% SDS-PAGE gels and transferred to PVDF membranes. The individual blots were blocked with 5% nonfat milk for 1 hr and stained overnight with specific antibodies; TRAF3 H-122 (Santa Cruz), NIK (Cell Signaling), cIAP1 (human) and cIAP2 (human) (R&D Systems), and NFKB2 (rabbit anti-p100/p52 N-terminal polyclonal, kindly provided by Warner Greene, UCSF). Protein bands of interest were imaged with HRP-conjugated secondary antibodies.

The localization of NFKB2 in HMCL and selected patient core biopsies was determined with an NFKB2 monoclonal antibody (18D10, Cell Signaling Technology). Fresh cytospins of HMCLs were fixed in 4% paraformaldeyde, permeabilized with 0.1% Triton X-100, and stained with a 1:50 dilution. Confocal slices of 2 μm were collected on a Zeiss LSM510 microscope using a 63× objective (Zeiss, Plan-Apochromat

63×/1.4 oil). Sections from available core biopsies were stained with a 1:50 dilution.

Generation of Helper-Dependent Adenoviral Vectors

We created a helper-dependent adenoviral (HDAd) vector precursor plasmid system capable of the simultaneous expression of EGFP and a gene-of-interest from two different promoters near the left and right ITRs, respectively. The original adenoviral plasmids, which have been described previously(Shi et al., 2006), were kindly provided by Mary Hitt (University of Alberta). First, we created the HDAd precursor plasmid, pSC27B, by replacing the beta-galactosidase expression cassette near the left ITR of pSC9B with a murine cytomegalovirus (mCMV)-driven EGFP expression cassette. Second, we created the pSC11MCPA shuttle plasmid by introducing a mCMV-MCS-SV40 poly-A cassette in between the I-SceI and I-CeuI restriction sites of pSC11. Thus, allowing a gene-of-interest expression cassette from pSC11MCPA to be transferred to a region near the right ITR of pSC27B.

The full-length TRAF3 cDNA clone (Image Consortium clone 30915387) was purchased from Open Biosystems. The ORF was excised from the pCR4.0-TOPO vector with EcoRI and cloned into the MCS of pSC11MCPA. The expression cassette was excised from pSC11MCPA-TRAF3 with I-CeuI and I-SceI and transferred to pSC27B to create pSC27B-TRAF3. Helper-dependent adenoviral particles were prepared by repeated cycles of amplification in 293Cre4 cells (kindly provided by Frank Graham, McMaster University) with the adeno helper virsus AdRP2050 (Robin Parks, Ottawa Health Research Institute), which contains a capsid modified by insertion of RGD into the H1 loop of the fiber. Virus particles were purified with a 1 hr step gradient and overnight continuous CsCl gradients as described previously (Parks et al., 1996). Virus particles were quantified as described previously (Ng et al., 2002). Healthy HMCLs were infected with 150 viral particles per cell in 60 mm Petri plates with 2.5×10^6 cells in 5 ml of antibiotic free media. The percentage of infected cells was monitored by FACS analysis of the coexpressed GFP marker.

Functional Analysis of TRAF3^{wt} Reintroduction

Infected HMCL were counted 24 hr postinfection and seeded at specific densities in triplicate in 96 well plates, for MTT assay, and 6 well dishes for protein assays, apoptosis, and cell-cycle analysis. For protein assays, TRAF3^{wt} and control infected cells were isolated 48 hr postinfection. For cell-cycle analysis, cells were stained with propidium iodide and the FACS results were modeled with ModFit LT and chi-square value below 5. The number of apoptotic cells was determined by Annexin-V-Alexa 647 (Invitrogen) staining.

Electronic Availability of the Data

A complete list of the patient samples and various tests are provided in Table S6. The publicly available data sets used in this paper are available in gene expression omnibus (GEO) or institutional websites as follows: Carrasco et al. GEP (GSE4452) and aCGH (http://genomic.dfci.harvard.edu/array_cgh_db.htm). The GEP data from our patient data set is available in the GEO database under the accession number GSE6477. The complete data set is freely available from the Multiple Myeloma Research Consortium Genomics Portal (http://www.broad.mit.edu/mmgp).

Supplemental Data

The Supplemental Data include 11 supplemental figures, six supplemental tables, and three supplemental data sets and can be found with this article online at http://www.cancercell.org/cgi/content/full/12/2/131/DC1/.

ACKNOWLEDGMENTS

We are indebted to Warner C. Green and Robin J. Parks for so kindly providing the anti-p100/p52 antibody and AdRP2050 helper adenovirus. We would also like to thank the TGen Sequencing Core facility for their assistance with the DNA sequencing. We would also like to thank Paige Anderson, Aprill Watanabe, and Sandra Montgomery for their invaluable assistance. This work was supported by grants R01-AG020686 (P.L.B.), R01-CA83724-01 (R.F.), SPORE P50-CA100707-01 (R.F. and P.L.B.) and P01-CA62242 (R.F.) from the National Cancer Institute, and the Donaldson Charitable Trust Fund (R.F.). R.F. is a Clinical Investigator of the Damon Runyon Cancer Research Fund. L.B. is an Agilent Biosciences employee. M.B. is a former Agilent Biosciences employee. B.B. and G.M. are employees of Millennium Pharmaceuticals. R.F. has a consulting agreement with Millennium Pharmaceuticals.

Received: January 19, 2007
Revised: May 9, 2007
Accepted: July 13, 2007
Published: August 13, 2007

REFERENCES

Barrett, M.T., Scheffer, A., Ben-Dor, A., Sampas, N., Lipson, D., Kincaid, R., Tsang, P., Curry, B., Baird, K., Meltzer, P.S., et al. (2004). Comparative genomic hybridization using oligonucleotide microarrays and total genomic DNA. Proc. Natl. Acad. Sci. USA *101*, 17765–17770.

Bergsagel, P.L., Chesi, M., Nardini, E., Brents, L.A., Kirby, S.L., and Kuehl, W.M. (1996). Promiscuous translocations into immunoglobulin heavy chain switch regions in multiple myeloma. Proc. Natl. Acad. Sci. USA *93*, 13931–13936.

Bergsagel, P.L., Kuehl, W.M., Zhan, F., Sawyer, J., Barlogie, B., and Shaughnessy, J., Jr. (2005). Cyclin D dysregulation: An early and unifying pathogenic event in multiple myeloma. Blood *106*, 296–303.

Caamano, J.H., Rizzo, C.A., Durham, S.K., Barton, D.S., Raventos-Suarez, C., Snapper, C.M., and Bravo, R. (1998). Nuclear factor (NF)-kappa B2 (p100/p52) is required for normal splenic microarchitecture and B cell-mediated immune responses. J. Exp. Med. *187*, 185–196.

Carrasco, D.R., Tonon, G., Huang, Y., Zhang, Y., Sinha, R., Feng, B., Stewart, J.P., Zhan, F., Khatry, D., Protopopova, M., et al. (2006). High-resolution genomic profiles define distinct clinico-pathogenetic subgroups of multiple myeloma patients. Cancer Cell *9*, 313–325.

Ciana, P., Neri, A., Cappellini, C., Cavallo, F., Pomati, M., Chang, C.C., Maiolo, A.T., and Lombardi, L. (1997). Constitutive expression of lymphoma-associated NFKB-2/Lyt-10 proteins is tumorigenic in murine fibroblasts. Oncogene *14*, 1805–1810.

Courtois, G., and Gilmore, T.D. (2006). Mutations in the NF-kappaB signaling pathway: Implications for human disease. Oncogene *25*, 6831–6843.

Dejardin, E. (2006). The alternative NF-kappaB pathway from biochemistry to biology: Pitfalls and promises for future drug development. Biochem. Pharmacol. *72*, 1161–1179.

Fonseca, R., Blood, E., Rue, M., Harrington, D., Oken, M.M., Kyle, R.A., Dewald, G.W., Van Ness, B., Van Wier, S.A., Henderson, K.J., et al. (2003a). Clinical and biologic implications of recurrent genomic aberrations in myeloma. Blood *101*, 4569–4575.

Fonseca, R., Debes-Marun, C.S., Picken, E.B., Dewald, G.W., Bryant, S.C., Winkler, J.M., Blood, E., Oken, M.M., Santana-Davila, R., Gonzalez-Paz, N., et al. (2003b). The recurrent IgH translocations are highly associated with nonhyperdiploid variant multiple myeloma. Blood *102*, 2562–2567.

Fotin-Mleczek, M., Henkler, F., Hausser, A., Glauner, H., Samel, D., Graness, A., Scheurich, P., Mauri, D., and Wajant, H. (2004). Tumor necrosis factor receptor-associated factor (TRAF) 1 regulates CD40-induced TRAF2-mediated NF-kappaB activation. J. Biol. Chem. *279*, 677–685.

Fracchiolla, N.S., Lombardi, L., Salina, M., Migliazza, A., Baldini, L., Berti, E., Cro, L., Polli, E., Maiolo, A.T., and Neri, A. (1993). Structural alterations of the NF-kappa B transcription factor lyt-10 in lymphoid malignancies. Oncogene *8*, 2839–2845.

Franzoso, G., Carlson, L., Poljak, L., Shores, E.W., Epstein, S., Leonardi, A., Grinberg, A., Tran, T., Scharton-Kersten, T., Anver, M., et al. (1998). Mice deficient in nuclear factor (NF)-kappa B/p52 present with defects in humoral responses, germinal center reactions, and splenic microarchitecture. J. Exp. Med. *187*, 147–159.

Grech, A.P., Amesbury, M., Chan, T., Gardam, S., Basten, A., and Brink, R. (2004). TRAF2 differentially regulates the canonical and noncanonical pathways of NF-kappaB activation in mature B cells. Immunity *21*, 629–642.

He, J.Q., Zarnegar, B., Oganesyan, G., Saha, S.K., Yamazaki, S., Doyle, S.E., Dempsey, P.W., and Cheng, G. (2006). Rescue of TRAF3-null mice by p100 NF-kappa B deficiency. J. Exp. Med. *203*, 2413–2418.

He, J.Q., Saha, S.K., Kang, J.R., Zarnegar, B., and Cheng, G. (2007). Specificity of TRAF3 in its negative regulation of the noncanonical NF-kappa B pathway. J Biol Chem. *282*, 3688–3694. Published online December 11, 2006. 10.1074/jbc.M610271200.

Hoffmann, A., and Baltimore, D. (2006). Circuitry of nuclear factor kappaB signaling. Immunol. Rev. *210*, 171–186.

Ishikawa, H., Carrasco, D., Claudio, E., Ryseck, R.P., and Bravo, R. (1997). Gastric hyperplasia and increased proliferative responses of lymphocytes in mice lacking the COOH-terminal ankyrin domain of NF-kappaB2. J. Exp. Med. *186*, 999–1014.

Karin, M. (2006). Nuclear factor-kappaB in cancer development and progression. Nature *441*, 431–436.

Khaja, R., Zhang, J., Macdonald, J.R., He, Y., Joseph-George, A.M., Wei, J., Rafiq, M.A., Qian, C., Shago, M., Pantano, L., et al. (2006). Genome assembly comparison identifies structural variants in the human genome. Nat. Genet. *38*, 1413–1418.

Kuai, J., Nickbarg, E., Wooters, J., Qiu, Y., Wang, J., and Lin, L.L. (2003). Endogenous association of TRAF2, TRAF3, cIAP1, and Smac with lymphotoxin beta receptor reveals a novel mechanism of apoptosis. J. Biol. Chem. *278*, 14363–14369.

Kuehl, W.M., and Bergsagel, P.L. (2002). Multiple myeloma: Evolving genetic events and host interactions. Nat. Rev. Cancer *2*, 175–187.

Liao, G., Zhang, M., Harhaj, E.W., and Sun, S.C. (2004). Regulation of the NF-kappaB-inducing kinase by tumor necrosis factor receptor-associated factor 3-induced degradation. J. Biol. Chem. *279*, 26243–26250.

Mulligan, G., Mitsiades, C., Bryant, B., Zhan, F., Chng, W.J., Roels, S., Koenig, E., Fergus, A., Huang, Y., Richardson, P., et al. (2007). Gene expression profiling and correlation with outcome in clinical trials of the proteasome inhibitor bortezomib. Blood *109*, 3177–3188. Published online December 21, 2006. 10.1182/blood-2006-09-044974.

Neri, A., Chang, C.C., Lombardi, L., Salina, M., Corradini, P., Maiolo, A.T., Chaganti, R.S., and Dalla-Favera, R. (1991). B cell lymphoma-associated chromosomal translocation involves candidate oncogene lyt-10, homologous to NF-kappa B p50. Cell *67*, 1075–1087.

Ng, P., Parks, R.J., and Graham, F.L. (2002). Preparation of helper-dependent adenoviral vectors. Methods Mol. Med. *69*, 371–388.

Olshen, A.B., Venkatraman, E.S., Lucito, R., and Wigler, M. (2004). Circular binary segmentation for the analysis of array-based DNA copy number data. Biostatistics *5*, 557–572.

Parks, R.J., Chen, L., Anton, M., Sankar, U., Rudnicki, M.A., and Graham, F.L. (1996). A helper-dependent adenovirus vector system: Removal of helper virus by Cre-mediated excision of the viral packaging signal. Proc. Natl. Acad. Sci. USA *93*, 13565–13570.

Qing, G., Qu, Z., and Xiao, G. (2005). Stabilization of basally translated NF-kappaB-inducing kinase (NIK) protein functions as a molecular switch of processing of NF-kappaB2 p100. J. Biol. Chem. *280*, 40578–40582.

Rajkumar, S.V., Richardson, P.G., Hideshima, T., and Anderson, K.C. (2005). Proteasome inhibition as a novel therapeutic target in human cancer. J. Clin. Oncol. *23*, 630–639.

Redon, R., Ishikawa, S., Fitch, K.R., Feuk, L., Perry, G.H., Andrews, T.D., Fiegler, H., Shapero, M.H., Carson, A.R., Chen, W., et al. (2006). Global variation in copy number in the human genome. Nature *444*, 444–454.

Richardson, P.G., Barlogie, B., Berenson, J., Singhal, S., Jagannath, S., Irwin, D., Rajkumar, S.V., Srkalovic, G., Alsina, M., Alexanian, R., et al. (2003). A Phase 2 Study of Bortezomib in Relapsed, Refractory Myeloma. N. Engl. J. Med. *348*, 2609–2617.

Sen, R. (2006). Control of B lymphocyte apoptosis by the transcription factor NF-kappaB. Immunity *25*, 871–883.

Shi, C.X., Graham, F.L., and Hitt, M.M. (2006). A convenient plasmid system for construction of helper-dependent adenoviral vectors and its application for analysis of the breast-cancer-specific mammaglobin promoter. J. Gene Med. *8*, 442–451.

Shinkura, R., Kitada, K., Matsuda, F., Tashiro, K., Ikuta, K., Suzuki, M., Kogishi, K., Serikawa, T., and Honjo, T. (1999). Alymphoplasia is caused by a point mutation in the mouse gene encoding Nf-kappa b-inducing kinase. Nat. Genet. *22*, 74–77.

Vischioni, B., Giaccone, G., Span, S.W., Kruyt, F.A., and Rodriguez, J.A. (2004). Nuclear shuttling and TRAF2-mediated retention in the cytoplasm regulate the subcellular localization of cIAP1 and cIAP2. Exp. Cell Res. *298*, 535–548.

Zapata, J.M., Krajewska, M., Krajewski, S., Kitada, S., Welsh, K., Monks, A., McCloskey, N., Gordon, J., Kipps, T.J., Gascoyne, R.D., et al. (2000). TNFR-associated factor family protein expression in normal tissues and lymphoid malignancies. J. Immunol. *165*, 5084–5096.

Accession Numbers

The GEP data from our patient data set are available in the GEO database under the accession number GSE6477.